

Competing shape evolution, crossing configurations and single particle levels in nuclei

N. Gavrielov*

GANIL, CEA/DSM-CNRS/IN2P3, Bd Henri Becquerel, BP 55027, F-14076 Caen Cedex 5, France and
Racah Institute of Physics, The Hebrew University, Jerusalem 91904, Israel

(Dated: October 8, 2024)

The evolution of shape in the even-even zirconium (Zr) isotopes has been the subject of study for many years. However, the odd-mass isotopes have not been investigated as extensively due to limited experimental accessibility and computational challenges. This work, employing the interacting boson-fermion model with configuration mixing, examines the effect of rapid shape evolution and normal-intruder configuration crossing — both identified as quantum phase transitions — alongside evolution in single particle energies, on the positive-parity spectrum of odd-mass $^{93-103}\text{Zr}$ isotopes. Calculated energy levels, magnetic moments, $B(E2)$ values, and quadrupole moments are compared to experimental data, showing good agreement. The special case of ^{99}Zr , which lies near the critical point of both quantum phase transitions, is also addressed, offering a new interpretation to the $7/2_1^+$ isomeric state and the occurrence of the type II shell evolution, in light of recent debates.

The study of atomic nuclei reveals a diverse array of phenomena, from single particle excitations to collective motions and shape coexistence. These phenomena are crucial for understanding the evolution of nuclear structure across different isotopes. In particular, the evolution of effective single particle energies (ESPE) and the resulting formation of collective bands [1] provide insight into the interplay between nucleon interactions and nuclear shape changes.

Often, the evolution in shapes discloses a quantum phase transition (QPT) [2] that is apparent in the spectrum, where the shape is the phase that changes as one varies the control parameter, the number of nucleons (A). Furthermore, coexisting shapes have been studied extensively, and are shown to occur due to particle-hole excitations across multiple shell model configuration [3]. In certain cases, these configurations can cross, leading to a different kind of QPT [4] with the phase being the dominant shell model configuration in the ground state wave function.

The scenario of configuration crossing QPT is rather unique and was identified in the even-even zirconium (Zr) isotopes, attributed to proton-neutron interactions within spin-orbit partner orbitals [5], i.e. orbitals with $j_\pi = \ell \pm 1/2$ and $j_\nu = \ell \mp 1/2$. Subsequent studies found that such spin-orbit partners can cause a type II shell evolution of the EPSEs, influencing the QPT [6].

The effect of single particle degrees of freedom is even more accentuated in odd-mass nuclei, where the nucleus can be viewed as an even-even core coupled to an extra fermion. Nevertheless, theoretical investigations of odd-mass nuclei, remain limited. This gap is particularly evident in the study of odd-Zr isotopes, where previous works mentioned the need for incorporating configuration

mixing [7–13].

Recent studies have demonstrated that the configuration crossing QPT in the even-even Zr isotopes is intertwined with a shape-evolution QPT, leading to a scenario termed intertwined QPTs (IQPTs) [14–16]. Subsequently, using the new interacting boson-fermion model with configuration mixing (IBFM-CM) [17], the spectrum of odd-mass niobium (Nb) isotopes also revealed the occurrence of IQPTs [17, 18]. This underscored the necessity of incorporating multiple configurations to fully understand the structure of odd-mass nuclei.

The odd $^{93-103}\text{Zr}$ isotopes exhibit a rapid change in ground state total angular momentum: $5/2^+$, $5/2^+$, $1/2^+$, $1/2^+$, $3/2^+$, and $5/2^-$. This change, caused by neutron orbit occupations that shift the Fermi level, is key to understanding the behavior of these isotopes. In heavier Zr isotopes, the evolving single quasi-particle energies (SqPEs) affect the spectrum. The SqPEs evolution, driven also by the configuration crossing QPT and shape evolution QPT within the even-even Zr core [16], contrasts with the Nb isotopes study [17, 18], where the Fermi level remains unchanged.

It is therefore the goal of this paper to unravel the effect on the spectrum and the interplay between the triad evolution of shapes, configurations, and single quasi-particle energies in the odd $^{93-103}\text{Zr}$ isotopes.

The IBFM-CM is employed to study odd- A nuclei [17, 18]. In the IBFM [19], a boson core represents the adjacent even-even nuclei and is coupled to a fermion (a). The core is described using the interacting boson model with configuration mixing [20–22], where N_b monopole (s) and quadrupole (d) bosons represent 0p-0h excitations and 2p-2h core excitations with $N_b + 2$ bosons. The total Hamiltonian can be written in the form of

$$\hat{H} = \hat{H}_b + \hat{H}_f + \hat{H}_{bf} = \begin{bmatrix} \hat{H}_b^A(\eta^{(A)}) & \hat{V}_b(\omega) \\ \hat{V}_b(\omega) & \hat{H}_b^B(\eta^{(B)}) \end{bmatrix} + \begin{bmatrix} \sum_j \epsilon_j \hat{n}_j & 0 \\ 0 & \sum_j \epsilon_j \hat{n}_j \end{bmatrix} + \begin{bmatrix} \hat{H}_{bf}^A(\zeta^{(A)}) & 0 \\ 0 & \hat{H}_{bf}^B(\zeta^{(B)}) \end{bmatrix}, \quad (1)$$

In Eq. (1), \hat{H}_b represents the boson Hamiltonian. Here,

$\hat{H}_b^A(\eta^{(A)})$ describes the normal A configuration with N_b

bosons, while $\hat{H}_b^A(\eta^{(A)})$ describes the intruder B configuration with $N_b + 2$ bosons. Here, a typical Hamiltonian for both configurations is used

$$\hat{H}_b^i = \epsilon_d^{(i)} \hat{n}_d + \kappa^{(i)} \hat{Q}_\chi \cdot \hat{Q}_\chi + \kappa'^{(i)} \hat{L} \cdot \hat{L} + \delta_{i,B} \Delta_b, \quad (2)$$

with $i = A, B$. Interactions in Eq. (2) include the d -bosons number operator $\hat{n}_d = \sqrt{5}(\hat{d}^\dagger \hat{d})^{(0)}$, the rotational term $\hat{L} = \sqrt{10}(\hat{d}^\dagger \hat{d})^{(0)}$, and the quadrupole operator

$$\hat{Q}_\chi = (d^\dagger s + s^\dagger \tilde{d})^{(2)} + \chi(d^\dagger \tilde{d})^{(2)}, \quad (3)$$

where s and d are spherical tensors, coupled in a tensor product and $\tilde{d}_\mu = (-)^\mu d_{-\mu}$. The parameter Δ_b represents the energy offset between configurations A and B, and the mixing term \hat{V}_b is given by

$$\hat{V}_b = \omega[(d^\dagger d^\dagger)^{(0)} + (s^\dagger)^2] + \text{H.c.}, \quad (4)$$

where H.c. stands for Hermitian conjugate.

For \hat{H}_f , the fermion Hamiltonian, $\hat{n}_j = \sum_\mu a_{j\mu}^\dagger a_{j\mu}$ is the fermion number operator, with ϵ_j as single particle energies for each orbit and j the angular momentum of the orbital.

The Bose-Fermi Hamiltonian \hat{H}_{bf} consists of monopole, quadrupole, and exchange terms with respective strengths $A_0^{(i)}, \Gamma_0^{(i)}$, and $\Lambda_0^{(i)}$ ($i = A, B$), and occupation probabilities (u_j, v_j) following the microscopic interpretation of the IBFM [18].

After diagonalization, the resulting wave functions are of the form

$$\begin{aligned} |\Psi; J\rangle = & \sum_{\alpha, L, j} C_{\alpha, L, j}^{(N, J)} |\Psi_A; [N_b], \alpha, L, j; J\rangle \\ & + \sum_{\alpha, L, j} C_{\alpha, L, j}^{(N+2, J)} |\Psi_B; [N_b+2], \alpha, L, j; J\rangle, \end{aligned} \quad (5)$$

Here, N_b is the boson number, α the quantum numbers from the boson Hamiltonian, L (j) the boson (fermion) angular momentum, and J the total angular momentum. The occupation probabilities for the boson number N_b , the n_d boson number, and the single particle orbitals of the wave function can be determined from

$$v_{(N_i, J)}^2 = \sum_{n_d} v_{n_d; (N_i, J)}^2 = \sum_j v_{j; (N_i, J)}^2, \quad i = A, B \quad (6a)$$

$$v_{(j; N_i, J)}^2 = \sum_{\alpha, L} |C_{\alpha, L, j}^{(N_i, J)}|^2, \quad (6b)$$

$$v_{(n_d; N_i, J)}^2 = \sum_{\tau, n_\Delta, j, L} |C_{n_d, \tau, n_\Delta, L, j}^{(N_i, J)}|^2. \quad (6c)$$

For Eq. (6a), $v_{(N_A, J)}^2 + v_{(N_B, J)}^2 = 1$, where $N_A = N_b, N_B = N_b + 2$. It provides the occupation probability of N_b , indicating the proportion of normal ($v_{(N_A, J)}^2$)

and intruder ($v_{(N_B, J)}^2$) configurations. Eq. (6b) represents the occupation probability of the single particle orbitals, j . Eq. (6c) represents the occupation probability of n_d , which indicates the degree of deformation. A large $v_{(n_d; N_i, J)}^2$ suggests dominant U(5) boson symmetry, equivalent to a spherical shape (phase) in the geometrical interpretation of the IBM [20]. If the wave function is distributed among several n_d values, it indicates deformation. Thus, using Eqs. (6a) to (6c) one can analyze the evolution of occupation in the configurational, single particle and deformation content of the wave functions.

To analyze electromagnetic transitions, the operator with multipolarity L for transitions of type σ is defined as

$$\hat{T}(\sigma L) = \hat{T}_b(\sigma L) + \hat{T}_f(\sigma L), \quad (7)$$

with boson $\hat{T}_b(\sigma L)$ and fermion $\hat{T}_f(\sigma L)$ parts. In this work, we concentrate on $E2$ and $M1$ transitions

$$\hat{T}_b(E2) = e^{(A)} \hat{Q}_\chi^{(N)} + e^{(B)} \hat{Q}_\chi^{(N+2)}, \quad (8a)$$

$$\hat{T}_f(E2) = \sum_{jj'} f_{jj'}^{(2)} [a_j^\dagger \times \tilde{a}_{j'}]^{(2)}, \quad (8b)$$

$$\begin{aligned} \hat{T}_b(M1) = & \sum_i \sqrt{\frac{3}{4\pi}} g^{(i)} \hat{L}^{(N_i)} \\ & + \tilde{g}^{(i)} [\hat{Q}_\chi^{(N_i)} \times \hat{L}^{(N_i)}]^{(1)}. \end{aligned} \quad (8c)$$

$$\hat{T}_f(M1) = \sum_{jj'} f_{jj'}^{(1)} [a_j^\dagger \times \tilde{a}_{j'}]^{(1)}. \quad (8d)$$

For the $E2$ transitions, Eq. (8a) defines the boson effective charges for configurations A and B as $e^{(A)}$ and $e^{(B)}$, respectively. In Eq. (8b), the fermion part is given by $f_{jj'}^{(2)} = -\frac{e_f}{\sqrt{5}} \langle j | Y_{lm}^{(2)} | j' \rangle$, where e_f is the fermion effective charge.

For the $M1$ transitions, Eq. (8c) specifies the free value of the neutron spin g -factor as $g_s = -3.8263 \mu_N$, which is quenched by 30%, while the orbital angular momentum g -factor is $g_l = 0 \mu_N$.

The ^{40}Zr isotopes with mass number $A = 93\text{--}103$ are described by coupling a neutron to their respective even-even ^{40}Zr cores with $A = 92\text{--}102$. The parameters of \hat{H}_b in Eq. (1) and the boson numbers are thus taken from a previous work [16], with the sign one χ in Eq. (3) modified for $^{92\text{--}96}\text{Zr}$, as recent measurements of spectroscopic quadrupole moments of ^{94}Zr have shown to be positive [23].

In the odd ^{40}Zr isotopes, the valence neutrons occupy different orbits within the $Z = 50\text{--}82$ shell. Talmi [24] showed that neutrons in $^{90\text{--}96}\text{Zr}$ primarily reside in the $\nu 1d_{5/2}$ orbital, with ^{96}Zr representing a subshell closure. Therefore, for $^{93\text{--}95}\text{Zr}$, an occupation of $n/(2j+1) = 3/6$ and $5/6$, respectively, is assumed, where n is the number of valence neutrons. For $^{97\text{--}103}\text{Zr}$, a BCS calculation is performed [18] to evaluate the SqPEs (ϵ_j) and their occupations (v_j^2). As more neutrons are added, the changing

TABLE I. Single quasi-particle occupations, the Fermi energy λ_F , and parameters in MeV of the boson-fermion interactions, $\hat{H}_{\text{bf}}^{(i)}$ of Eq. (1), obtained from a fit assuming $A_0^{(i)} = A_0$, $\Gamma_0^{(i)} = \Gamma_0$ and $\Lambda_0^{(i)} = \Lambda_0$ for $i = \text{A}$ and B . Beneath each isotope the number of valence neutrons used in the shell model ($^{93,95}\text{Zr}$) and BCS ($^{97-103}\text{Zr}$) evaluations is listed.

Isotope	^{93}Zr	^{95}Zr	^{97}Zr	^{99}Zr	^{101}Zr	^{103}Zr
# particles	3	5	1	3	5	7
$v_{\nu 1d_{5/2}}^2$	3/6	5/6	0	0	0	0
$v_{\nu 2s_{1/2}}^2$	0	0	0.085	0.351	0.567	0.697
$v_{\nu 1d_{3/2}}^2$	0	0	0.037	0.110	0.189	0.275
$v_{\nu 0g_{7/2}}^2$	0	0	0.033	0.091	0.152	0.219
$v_{\nu 0h_{11/2}}^2$	0	0	0.034	0.095	0.158	0.229
λ_F	0	0	-1.339	-0.281	0.122	0.385
A_0	-0.252	0.983	-0.367	-0.150	-0.146	0.133
Γ_0	0.037	0.086	0.059	0.455	0.464	0.757
Λ_0	1.191	1.063	1.121	1.910	1.910	1.824

Fermi energy affects these evaluations. According to the microscopic interpretation of the IBFM [25], the ϵ_j are required for \hat{H}_f , and v_j^2 impact \hat{H}_{bf} of Eq. (1). The neutrons are distributed among the $\nu 2s_{1/2}$, $\nu 1d_{3/2}$, $\nu 0g_{7/2}$, and $\nu 0h_{11/2}$ orbitals, with the $\nu d_{5/2}$ considered closed, as done in a previous IBFM calculation [26]. For the BCS calculation, the single particle energies of ^{91}Zr are used [27], along with a pairing gap of $\Delta_F = 0.9$ MeV, calculated as the average of $\Delta_F = \frac{1}{4}(B(N-2, Z) - 3B(N-1, Z) + 3B(N, Z) - B(N+1, Z))$ [28].

Table I presents the resulting v_j^2 and the strengths (A_0, Γ_0, Λ_0) for the positive-parity states. The strengths for the negative-parity states will be addressed in a subsequent publication. The exchange strength Λ_0 increases gradually along the isotopic chain. The quadrupole strength Γ_0 remains relatively constant for $^{93-97}\text{Zr}$ and $^{99-103}\text{Zr}$, suggesting an increase in deformation between these regions. The monopole strength A_0 decreases from ^{93}Zr to ^{101}Zr , with exceptions at ^{95}Zr and ^{103}Zr , possibly due to the lack of experimental data. The occupation probabilities increase with the number of valence neutrons, which in turn influences the SqPEs. The evolution in SqPEs, shown in Fig. 2(a), depicts a significant lowering of the $\nu 0h_{11/2}$, $\nu 0g_{7/2}$ and $\nu 1d_{3/2}$ orbitals from ^{97}Zr to ^{103}Zr .

The trends in strengths and SqPEs are reflected in the spectrum of $^{93-103}\text{Zr}$ isotopes, shown in Fig. 1, illustrating the energies of selected states. The calculated panel, showing good agreement with the experimental data, depicts the normal-intruder mixing, where filled (empty) symbols represent normal (intruder) states, as defined by Eq. (6a). For the lowest positive-parity state, the total angular momentum undergoes an intricate evolution: $5/2^+$ for $^{93,95}\text{Zr}$, $1/2^+$ for $^{97,99}\text{Zr}$, and $3/2^+$ for $^{101,103}\text{Zr}$.

This evolution results from a combination of deformation, configuration mixing, and single quasi-particle occupation. For $^{93,95}\text{Zr}$, the $5/2_1^+$ state results from the $\nu 1d_{5/2}$ orbital weakly coupled to the respective $^{92,94}\text{Zr}$ cores, particularly the spherical normal 0_1^+ . A similar situation occurs for $^{97,99}\text{Zr}$, where the $1/2_1^+$ state is associated with coupling the $\nu 2s_{1/2}$ orbital to the $^{96,98}\text{Zr}$ cores. For $^{101,103}\text{Zr}$, the $3/2_1^+$ state results from closely spaced orbitals, ontop of the onset of deformation and configuration crossing, where all the lowest lying states are intruder.

In Fig. 1 the lowest negative-parity level, J_{low}^- , and its configuration content is also shown. For $^{93,95}\text{Zr}$ it is $11/2^-$ normal, for ^{97}Zr it is $11/2^-$ intruder, for ^{99}Zr $7/2^-$ intruder, and for $^{101,103}\text{Zr}$ it is $5/2^-$ intruder (more details will be published elsewhere).

The analysis above is further stressed in Fig. 2, depicting the resulting SqPEs from the BCS calculation (panel a), and the different occupations of the lowest positive-parity state, J_{low}^+ : the SqP occupation (6b) (panel b), $n_d\text{-U}(5)$ boson symmetry occupation (6c) (panel c) and configuration content (6a) (panel d).

For $^{93,95}\text{Zr}$, panel (b) shows a dominant $\nu 1d_{5/2}$ orbit, panel (c) shows a dominant $n_d = 0$ component, and panel (d) shows a dominant normal component. This indicates a weak coupling scenario of a normal wave function with good $\text{U}(5)$ boson symmetry coupled to a $\nu 1d_{5/2}$ orbital. A similar pattern is observed for $^{97,99}\text{Zr}$, but with the $\nu 2s_{1/2}$ orbital instead. In contrast, for $^{101,103}\text{Zr}$, panel (b) shows a mixture of $\nu 2s_{1/2}$, $\nu 1d_{3/2}$ and $\nu 0g_{7/2}$ orbitals within the intruder part of the wave function, panel (c) shows boson $\text{U}(5)\text{-}n_d$ occupations indicating a deformed intruder state, and panel (d) shows almost no normal occupation in the wave function, indicating an almost pure intruder state.

The increase in j -mixture observed in panel (b) corresponds clearly to the lowering of the SqPEs shown in (a) of Fig. 2. The evolution observed in panels (c) and (d), from spherical to deformed states and from normal to intruder configurations, indicates the presence of the two quantum phase transitions (IQPTs) similar to those seen in the even-even Zr and odd-mass Nb chains [29].

To further examine the calculated wave functions, it is essential to compare them with electromagnetic transition rates. For $E2$ transitions in Eq. (8), the boson effective charges $e^{(\text{A})}, e^{(\text{B})}$ are taken from [16]. The fermion effective charge, $e_f = 3.258 \sqrt{\text{W.u.}}$, is determined from a fit to the spectroscopic quadrupole moment of ^{95}Zr , $Q_{5/2_1^+} = 0.22(2) \text{ eb}$.

The fitting procedure yields $Q_{3/2_1^+} = 0.27 \text{ eb}$ for ^{101}Zr , compared to the experimental value of $Q = 0.81(6) \text{ eb}$. The experimental $E2$ transitions (calculation in parentheses) are: ^{93}Zr : $B(E2; 3/2_1^+ \rightarrow 5/2_1^+) = 6.6(23) \text{ W.u.}$ (1.1), ^{97}Zr : $B(E2; 7/2_1^+ \rightarrow 3/2_1^+) = 1.55(5) \text{ W.u.}$ (4.80), ^{99}Zr : $B(E2; 7/2_1^+ \rightarrow 3/2_1^+) = 1.33(5) \text{ W.u.}$ (1.91), and

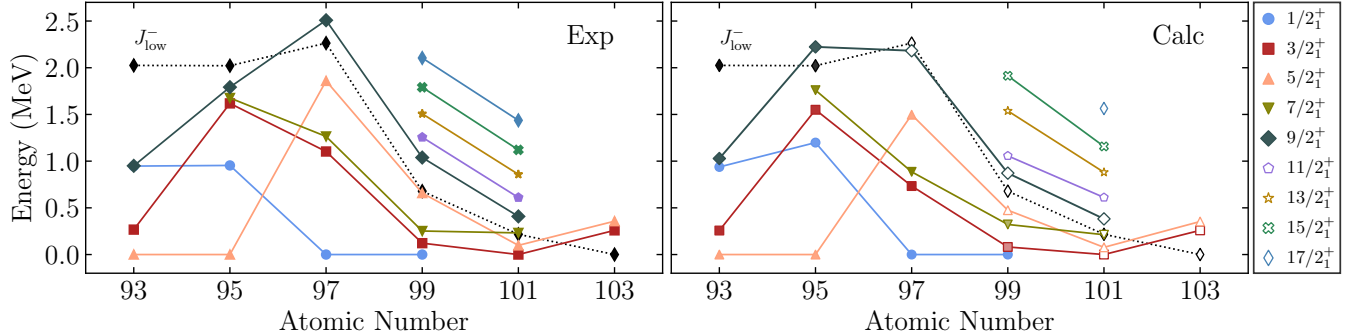


FIG. 1. Comparison between experimental (left panel) and calculated (right panel) lowest-energy levels in odd Zr isotopes. On the right panel, the symbols filling indicates the dominance of the normal A configuration (filled) or intruder B configuration (empty) with assignments based on Eq. (6a). For example, the $3/2_1^+$ is normal A configuration for $A = 93\text{--}97$, mixed for $A = 99$, and intruder B configuration for $A = 101\text{--}103$.

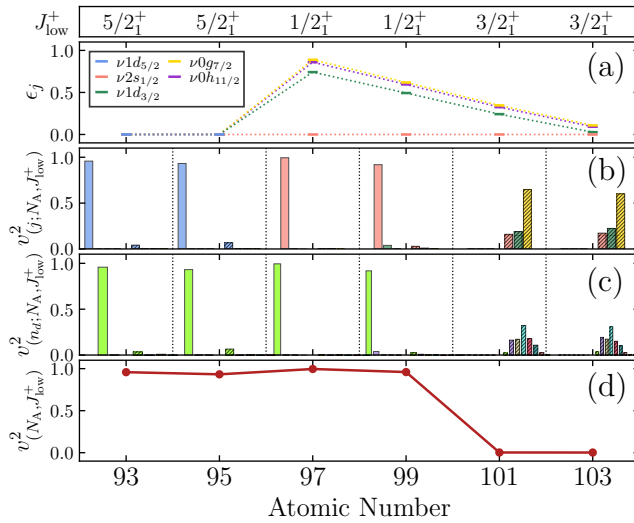


FIG. 2. Evolution of: (a) Single quasi-particle energies, ϵ_j ; (b) Single quasi-particle occupation probabilities of the lowest positive-parity state, J_{low}^+ , Eq. (6b). Each color indicates a different orbital: $\nu 1d_{5/2}$ (blue), $\nu 0g_{7/2}$ (yellow), $\nu 2s_{1/2}$ (red), $\nu 0h_{11/2}$ (green). Note the transition from a singular single quasi-particle occupation for $^{93\text{--}99}\text{Zr}$ to a distribution of them for $^{101\text{--}103}\text{Zr}$; (c) n_d occupation probability of the lowest positive-parity state, J_{low}^+ , Eq. (6c), depicting the different possible normal ($n_d = 0, \dots, N_b$) and intruder ($n_d = 0, \dots, N_b + 2$) n_d values. Each color represents a different n_d number from $n_d = 0$ (green) to $n_d = 8$ (blue). Note the transition from a single dominant bar (representing a spherical state) for $^{93\text{--}99}\text{Zr}$ to a distribution of them (representing a deformed state) for $^{101\text{--}103}\text{Zr}$. In both (b) and (c), bars from the left (right) of the mass number correspond to normal (intruder) occupations, with intruder bars filled with diagonal lines; (d) the amount of normal occupation in the wave function, Eq. (6a). Note the transition from normal in $^{93\text{--}99}\text{Zr}$ to intruder in $^{101\text{--}103}\text{Zr}$. The values of J_{low}^+ are indicated in the uppermost panel.

^{101}Zr : $B(E2; 7/2_1^+ \rightarrow 3/2_1^+) > 130$ W.u. (82). The calculated values are reasonably close to the experimental

ones and indicate the onset of deformation at ^{101}Zr , as evidenced by the strong increase in transition strength, with a possible need for more deformation.

Magnetic moments, which are strongly influenced by the single particle structure, provide further indicative observables. For $M1$ transitions operator, Eq. (8), the same values for $g^{(A)}, g^{(B)}, \tilde{g}^{(A)}, \tilde{g}^{(B)}$ is used as in [17]. Fig. 3 compares the calculated magnetic moments with the experimental ones, as well as the single particle estimations [30]. For $^{95\text{--}99}\text{Zr}$, there is a good agreement between the calculation and experimental data for the ground state. Notably, the IBFM-CM result also coincides with the single particle estimations [30], further supporting the single particle character of the ground state. This interpretation extends to the $7/2_1^+$ state of ^{97}Zr , which exhibits an almost pure $\nu 0g_{7/2}$ occupation and spherical normal configuration in its wave function.

However, deviations from the single particle interpretation are observed for the excited states of ^{99}Zr and the ground state of ^{101}Zr . For the $3/2_1^+$ and $7/2_1^+$ states in these isotopes, better agreement is achieved with the IBFM-CM calculation. The reason is that these states become more mixed in their orbitals, losing their single quasi-particle character due to the onset of deformation and configuration mixing. In ^{99}Zr , the $3/2_1^+$ and $7/2_1^+$ are strongly mixed in configuration and n_d occupations. For the $7/2_1^+$, there is still some deviation for the IBFM-CM, which might suggest more deformation is needed in the ^{98}Zr core, as was suggested in [31]. For ^{101}Zr , the $3/2_1^+$ state is pure intruder deformed, with mixed orbitals, which explains the deviation from the single particle value.

A closer examination of ^{99}Zr is intriguing, as it lies nearest to the critical points of the shape evolution and configuration crossing QPTs between ^{98}Zr and ^{100}Zr [16]. Recently, an IBFM calculation with a single configuration was presented in [10, 11] for ^{99}Zr . In [11], the authors compared the $7/2_1^+$ state in ^{99}Zr to that in ^{97}Zr , noting

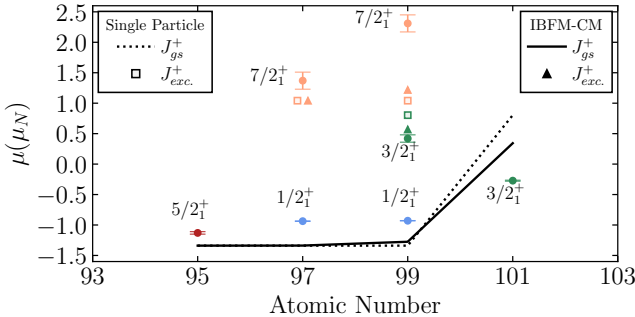


FIG. 3. Evolution of magnetic moments μ in units of μ_N , along the odd Zr chain. Symbols denote experimental data for the ground state and excited states when available, taken from [32]. Each J value has a different color. The solid (dashed) line and black triangles (squares) denote calculated results, based on Eqs. (8c) and (8d) (single particle estimation). See text for more details.

that both states are isomers. However, for the $7/2_1^+$ state, the magnetic moment for ^{99}Zr , $\mu_{7/2+1} = 2.31 (14) \mu_N$, deviates from the single particle prediction observed in ^{97}Zr . This led the authors in [11] to suggest the occurrence of a type II shell evolution, causing the *single particle* $\nu 2s_{1/2}$ orbital to become lower than the $\nu 1d_{5/2}$.

While Ref. [11] successfully reproduced this magnetic moment value, the calculated energies did not align well with experimental data. This discrepancy was later questioned in Ref. [33], leading the authors to propose an IBFM configuration mixing model for improvement. In [33], it was argued that there is no need for a change in the single particle energies, as suggested by previous works [7, 26]. Furthermore, as was suggested in [6], only the resulting *effective* single particle energies are modified, leading to the type II shell evolution between the spin orbit partners $\nu 0g_{7/2}$ and $\pi 0g_{9/2}$.

This work confirms that lowering the $\nu 2s_{1/2}$ single particle orbital is unnecessary in ^{99}Zr . Instead, the resulting single *quasi*-particle energies account for the $1/2_1^+$ state as a normal single *quasi*-particle state of the $\nu 2s_{1/2}$ orbital, while the $3/2_1^+$ and $7/2_1^+$ are mixed normal-intruder deformed states. Furthermore, the intruder character of the $7/2_1^+$ state in ^{99}Zr mainly results from coupling with the intruder 2_1^+ state of ^{98}Zr core (unlike the less conventional choice of ^{100}Zr boson core with a hole in [11]). Its isomeric nature is attributed to the dominant single *quasi*-particle component $\nu 0g_{7/2}$ in the normal-intruder components (total $v_{j=7/2_1^+}^2 = 0.86$), while for the $3/2_1^+$ state, it is the $\nu 1d_{3/2}$ orbital ($v_{j=3/2_1^+}^2 = 0.73$), which are weakly connected via $\hat{T}_f(E2)$ in Eq. (8). In ^{97}Zr , the isomeric nature arises from the single particle character of the 2_1^+ state of ^{96}Zr .

In summary, a comprehensive analysis of the odd $^{93-103}\text{Zr}$ isotopes has been conducted using the inter-

acting boson-fermion model with configuration mixing. This approach employed boson, fermion, and Bose-Fermi Hamiltonians with mixed configurations, focusing on positive-parity states. The good agreement with experimental data on energies, $E2$ transitions, and quadrupole and magnetic moments underscores the manifestation of shape, configuration, and single quasi-particle evolutions that influence the spectrum. The special case of ^{99}Zr was further examined in light of recent studies [10, 11] suggesting a type II shell evolution in the *single-particle* $\nu 2s_{1/2}$ orbit. It was demonstrated that while type II shell evolution occurs in the effective single particle orbits, as suggested in [6], it does not occur in the single particle orbits and does not lower the $\nu 2s_{1/2}$ orbit. Instead, the spectrum is shown to result from the interplay of shape, configuration, and single quasi-particle evolutions, offering a resolution to the recent debate [33, 34]. This work may inspire further experimental and theoretical efforts to identify and differentiate shape, configuration, and single particle effects in the structural evolution of atomic nuclei. As demonstrated here, these effects are particularly pronounced in odd-mass nuclei.

The author acknowledges support from the European Union's Horizon 2020 research and innovation program under the Marie Skłodowska-Curie grant agreement No. 101107805.

* noam.gavrielov@mail.huji.ac.il

- [1] T. Otsuka, Y. Tsunoda, T. Abe, N. Shimizu, and P. Van Duppen, *Phys. Rev. Lett.* **123**, 222502 (2019).
- [2] P. Cejnar, J. Jolie, and R. F. Casten, *Rev. Mod. Phys.* **82**, 2155 (2010).
- [3] K. Heyde and J. L. Wood, *Rev. Mod. Phys.* **83**, 1467 (2011).
- [4] A. Frank, P. Van Isacker, and F. Iachello, *Phys. Rev. C* **73**, 061302(R) (2006).
- [5] P. Federman and S. Pittel, *Phys. Rev. C* **20**, 820 (1979).
- [6] T. Togashi, Y. Tsunoda, T. Otsuka, and N. Shimizu, *Phys. Rev. Lett.* **117**, 172502 (2016).
- [7] S. Brant, V. Paar, and A. Wolf, *Phys. Rev. C* **58**, 1349 (1998).
- [8] G. Lhersonneau and S. Brant, *Phys. Rev. C* **72**, 034308 (2005).
- [9] R. Rodriguez-Guzman, P. Sarriguren, and L. M. Robledo, *Phys. Rev. C* **83**, 044307 (2011).
- [10] P. Spagnoletti, G. Simpson, S. Kishev, D. Bucurescu, J.-M. Régis, N. Saed-Samii, A. Blanc, M. Jentschel, U. Köster, P. Mutti, T. Soldner, G. de France, C. A. Ur, W. Urban, A. M. Bruce, C. Bernards, F. Drouet, L. M. Fraile, L. P. Gaffney, D. G. Ghita, S. Ilieva, J. Jolie, W. Korten, T. Kröll, S. Lalkovski, C. Larijarni, R. Lică, H. Mach, N. Mărginean, V. Paizy, Z. Podolyák, P. H. Regan, M. Scheck, J. F. Smith, G. Thiamova, C. Townsley, A. Vancraeyenest, V. Vedia, N. Warr, V. Werner, and M. Zielińska, *Phys. Rev. C* **100**, 014311 (2019).
- [11] F. Boulay, G. S. Simpson, Y. Ichikawa, S. Kishev, D. Bucurescu, A. Takamine, D. S. Ahn, K. Asahi, H. Baba,

D. L. Balabanski, T. Egami, T. Fujita, N. Fukuda, C. Funayama, T. Furukawa, G. Georgiev, A. Gladkov, M. Hass, K. Imamura, N. Inabe, Y. Ishibashi, T. Kawaguchi, T. Kawamura, W. Kim, Y. Kobayashi, S. Kojima, A. Kusoglu, R. Lozeva, S. Momiyama, I. Mukul, M. Niikura, H. Nishibata, T. Nishizaka, A. Odahara, Y. Ohtomo, D. Ralet, T. Sato, Y. Shimizu, T. Sumikama, H. Suzuki, H. Takeda, L. C. Tao, Y. Togano, D. Tominaga, H. Ueno, H. Yamazaki, X. F. Yang, and J. M. Daugas, *Phys. Rev. Lett.* **124**, 112501 (2020).

[12] K. Nomura, T. Nikšić, and D. Vretenar, *Phys. Rev. C* **102**, 034315 (2020).

[13] A. Pfeil, K. Nomura, N. Gavrielov, J.-M. Régis, U. Köster, Y. H. Kim, A. Esmaylzadeh, A. Harter, J. Jolie, L. Knafla, M. Ley, and V. Karayonchev, *Phys. Rev. C* **108**, 034310 (2023).

[14] N. Gavrielov, A. Leviatan, and F. Iachello, *Phys. Rev. C* **99**, 064324 (2019).

[15] N. Gavrielov, A. Leviatan, and F. Iachello, *Phys. Scr.* **95**, 024001 (2020).

[16] N. Gavrielov, A. Leviatan, and F. Iachello, *Phys. Rev. C* **105**, 014305 (2022).

[17] N. Gavrielov, A. Leviatan, and F. Iachello, *Phys. Rev. C* **106**, L051304 (2022).

[18] N. Gavrielov, *Phys. Rev. C* **108**, 014320 (2023).

[19] F. Iachello and P. Van Isacker, *The Interacting Boson-Fermion Model* (Cambridge University Press, 1991).

[20] F. Iachello and A. Arima, *The Interacting Boson Model* (Cambridge University Press, 1987).

[21] P. D. Duval and B. R. Barrett, *Phys. Lett. B* **100**, 223 (1981).

[22] P. D. Duval and B. R. Barrett, *Nucl. Phys. A* **376**, 213 (1982).

[23] N. Marchini, to be published (2024).

[24] I. Talmi, *Phys. Rev.* **126**, 2116 (1962).

[25] O. Scholten, *Prog. Part. Nucl. Phys.* **14**, 189 (1985).

[26] G. Lhersonneau, B. Pfeiffer, K. L. Kratz, H. Ohm, K. Sistemich, S. Brant, and V. Paar, *Zeitschrift für Phys. A At. Nucl.* **337**, 149 (1990).

[27] J. Barea and F. Iachello, *Phys. Rev. C* **79**, 044301 (2009).

[28] A. Bohr and B. R. Mottelson, *Nuclear structure*, Vol. 2 (World Scientific, 1998).

[29] N. Gavrielov, *Phys. Scr.* **99**, 075310 (2024).

[30] I. Talmi, *Simple Models of Complex Nuclei: The Shell Model and Interacting Boson Model* (Harwood Academic, 1993).

[31] V. Karayonchev, J. Jolie, A. Blazhev, A. Dewald, A. Esmaylzadeh, C. Fransen, G. Häfner, L. Knafla, J. Litzinger, C. Müller-Gatermann, J.-M. Régis, K. Schomacker, A. Vogt, N. Warr, A. Leviatan, and N. Gavrielov, *Phys. Rev. C* **102**, 064314 (2020).

[32] N. J. Stone, *At. Data Nucl. Data Tables* **90**, 75 (2005).

[33] P. E. Garrett, *Phys. Rev. Lett.* **127**, 169201 (2021).

[34] F. Boulay, G. S. Simpson, Y. Ichikawa, S. Kisoyev, D. Bucurescu, A. Takamine, D. S. Ahn, K. Asahi, H. Baba, D. L. Balabanski, T. Egami, T. Fujita, N. Fukuda, C. Funayama, T. Furukawa, G. Georgiev, A. Gladkov, M. Hass, K. Imamura, N. Inabe, Y. Ishibashi, T. Kawaguchi, T. Kawamura, W. Kim, Y. Kobayashi, S. Kojima, A. Kusoglu, R. Lozeva, S. Momiyama, I. Mukul, M. Niikura, H. Nishibata, T. Nishizaka, A. Odahara, Y. Ohtomo, D. Ralet, T. Sato, Y. Shimizu, T. Sumikama, H. Suzuki, H. Takeda, L. C. Tao, Y. Togano, D. Tominaga, H. Ueno, H. Yamazaki, X. F. Yang, and J. M. Daugas, *Phys. Rev. Lett.* **127**, 169202 (2021).